

Impact study for multi-girder bridge based on correlated road roughness

Chunhua Liu[†] and Ton-Lo Wang[‡]

Department of Civil and Environmental Engineering, Florida Int'l University, Miami, FL 33199, U.S.A.

Dongzhou Huang^{†‡}

*Structural Research Center, Florida Department of Transportation, 2007E,
Dirac Drive, Tallahassee, FL 32310, U.S.A.*

Abstract. The impact behavior of a multigirder concrete bridge under single and multiple moving vehicles is studied based on correlated road surface characteristics. The bridge structure is modeled as grillage beam system. A 3D nonlinear vehicle model with eleven degrees of freedom is utilized according to the HS20-44 truck design loading in the American Association of State Highway and Transportation Officials (AASHTO) specifications. A triangle correlation model is introduced to generate four classes of longitudinal road surface roughness as multi-correlated random processes along deck transverse direction. On the basis of a correlation length of approximately half the bridge width, the upper limits of impact factors obtained under confidence level of 95 percent and side-by-side three-truck loading provide probability-based evidence for the evaluation of AASHTO specifications. The analytical results indicate that a better transverse correlation among road surface roughness generally leads to slightly higher impact factors. Suggestions are made for the routine maintenance of this type of highway bridges.

Key words: highway bridge; road surface roughness; correlation analysis; dynamic analysis; impact study.

1. Introduction

Vehicle-induced impact on highway bridges is one of the primary problems concerning bridge engineers. The American Association of State Highway and Transportation Officials (AASHTO 1996) or AASHTO-LRFD (1998) specifications are the widely used design code to consider the live load impact. In lieu of the impact factor associated with span length, the AASHTO-LRFD specifications (1998) introduce the conception of dynamic load allowance *IM* based on various structural components and limit states. Numerous analytical and field studies have been conducted in this field to calibrate the impact factor specified by the AASHTO provisions. A brief review of these research works on simply supported short- and medium-span bridges refers to Fenves *et al.* (1962), Ruhl (1974), Wang *et al.* (1992), Huang *et al.* (1993), Wang *et al.* (1993), and Wang *et al.* (1996). In theoretical analyses, however, studies take little account of inherent spatial coherence among

[†] Assistant Scientist

[‡] Professor

^{†‡} Senior Scientist (Professor of Civ. and Arch. Eng., Fuzhou Univ., Fujian, China)

longitudinal road surface roughness along transverse bridge profile. In the sixties, Fenves *et al.* (1962) observed from field measurements that the permanent deflections along transverse bridge profiles increased with time. Law *et al.* (1975) measured and analyzed the transverse bridge profile differences related to wavelengths at three bridges. They concluded that the variation in transverse bridge profiles primarily came from various pavement types, wheelpath-to-wheelpath differences, and the lane-to-lane differences according to their contribution sequence. It is worthwhile to investigate in detail the possible discrepancy caused by different road roughness models.

The objective of this study is to evaluate the response characteristics of multigirder bridges based on spatially correlated longitudinal road surface roughness. A triangle correlation model for road surface roughness along transverse bridge profile is introduced in the analysis. On this basis, dynamic behavior of a multigirder concrete bridge with span length of 30.48 m, which is designed in accordance with AASHTO specifications (1996), is studied. The vehicle speeds range from 24.14 km/h to 120.70 km/h. To obtain statistical results, a total of twenty simulations is carried out for each study case with respect to road roughness class and vehicle speed. The influence of various correlation lengths on impact factors is investigated.

2. Bridge and HS20-44 models

2.1 Idealization of bridge structure

Fig. 1 shows a simply supported prestressed concrete highway bridge, which is designed according to AASHTO standard bridge girders (1996) and the Standard Plans for Highway Bridge Superstructures (1990) from the U.S. Department of Transportation. This bridge is made up of I-beam sections with a cast-in-place deck and is designed on the basis of HS20-44 loading. The bridge has a roadway width of 9.74 m and a concrete deck thickness of 0.19 m. Typical cross section of the bridge is shown in Fig. 1(a). All the five girders have identical section and are transversely connected with each other by diaphragms at two span third points and two span ends, as shown in the plan of the bridge in Fig. 1(b).

The multigirder bridge is treated as grillage beam system as shown in Fig. 2. Dynamic response of the bridge is analyzed with finite element method. The bridge is divided into grillage elements as shown in Fig. 3. The nodal parameters at element level are

$$\boldsymbol{\delta}^e = \begin{Bmatrix} \boldsymbol{\delta}_i \\ \boldsymbol{\delta}_j \end{Bmatrix} \quad (1)$$

where $\boldsymbol{\delta}_i = \{w_{zi}, \theta_{xi}, \theta_{yi}\}^T$ = displacement vector of the i th node; $\boldsymbol{\delta}_j = \{w_{zj}, \theta_{xj}, \theta_{yj}\}^T$ = displacement vector of the j th node; w = vertical displacement in the z -axis direction; and θ_x, θ_y = rotational displacements along x - and y -axis, respectively.

In the present study, rigidities of longitudinal elements are determined as composite sections consisting of girders and slab, while the stiffness of transverse elements consist of slab and diaphragm. The mass per length and crosssection of each girder are considered to be uniform along the longitudinal axis of the bridge. Table 1 presents the primary data of this bridge.

The equation of motion of the bridge is

$$\mathbf{M}_b \ddot{\boldsymbol{\delta}}_b + \mathbf{C}_b \dot{\boldsymbol{\delta}}_b + \mathbf{K}_b \boldsymbol{\delta}_b = \mathbf{F}_b \quad (2)$$

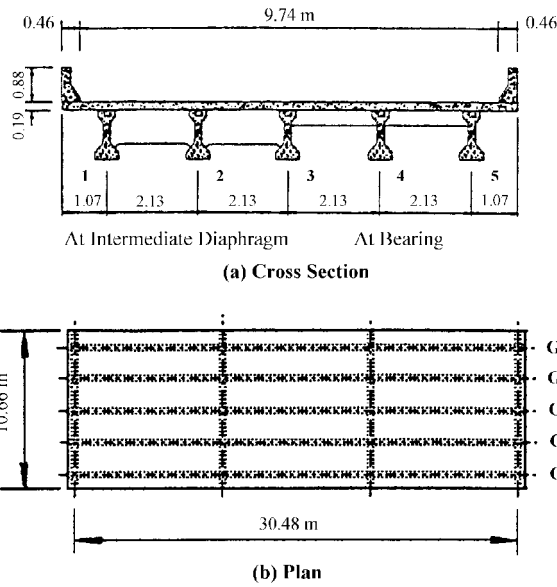


Fig. 1 Analytical bridge (in meters)

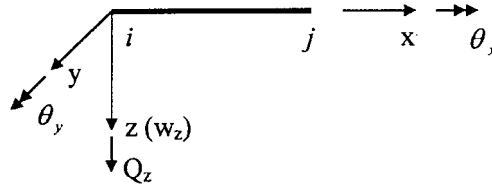


Fig. 2 Beam element

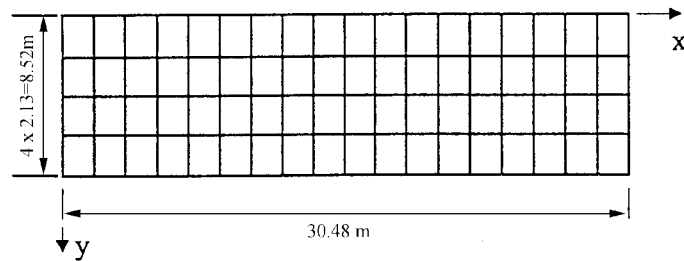


Fig. 3 Idealization of multigirder bridge

where M_b = global mass matrix of bridge structure; K_b = global stiffness matrix of bridge structure; C_b = global damping matrix of bridge structure; $\delta_b, \dot{\delta}_b, \ddot{\delta}_b$ = global nodal displacement, velocity, and acceleration vectors; and F_b = global load vector due to the interaction between bridge and vehicle.

3. HS20-44 model

The three-axle vehicle HS20-44 is the major design vehicle in the AASHTO specifications. A three-dimensional mathematical model for the HS20-44 truck loading is illustrated in Fig. 4. This

Table 1 Properties and masses of the bridge

Members (1)	Inertia moment I (m ⁴) (2)	Torsion inertia moment J_d (m ⁴) (3)	Mass (kN/m) (4)
Girder	0.26872	0.01363	27.07 ^a 22.43 ^b
Intermediate diaphragm	0.05777	0.007896	4.676
Diaphragm at ends	0.00718	0.005182	2.014

Note: a. Exterior girder; and b. Interior girder

model simplifies the standard truck into five rigid masses connected by six springs and six dampers. The five masses represent the tractor, semitrailer, steer-wheel/axle set, tractor wheel/axle set, and trailer wheel/axle set. There are a total of twelve assigned degrees of freedom (DOFs) shown in Fig. 4: three for tractor, three for semitrailer, and two for each wheel/axle set. The three DOFs for tractor and semitrailer include vertical displacement (z_t), rotation about the transverse axis (pitch or θ), and rotation about the longitudinal axis (roll or ϕ). Each wheel/axle set is assigned with two DOFs in the vertical and roll directions (z_t and ϕ). Since the tractor and the semitrailer are interconnected at the pivot point, namely fifth-wheel point (see Fig. 4), the total number of degrees of freedom is reduced to eleven. The equations of motion of the system were derived using Lagrange's equation. Details of derivation and data refer to Wang and Huang (1992).

3.1 Interaction between vehicle and bridge

The interaction force between the i th wheel of the vehicle and the bridge is given as following:

$$F_{bt}^i = K_{tzi} U_{tzi} + C_{tzi} \dot{U}_{tzi} \tag{3}$$

where K_{tzi} = tire stiffness of the i th wheel; C_{tzi} = tire damping coefficient of the i th wheel; $U_{tzi} = z_{wi} - (-u_{sri}) - (-z_{bi})$, the relative displacement between the i th wheel and bridge, and the superscript dot of U_{tzi} denotes differential with respect to time; z_{wi} = vertical displacement of the i th wheel; u_{sri} = road surface roughness under the i th wheel (positive upwards); and z_{bi} = bridge vertical displacement under the i th wheel (positive upwards), which can be determined by the nodal displacement δ^e and the displacement interpolation function of the element (Clough and Penzien 1996).

In the present study, the fourth-order Runge-Kutta integration algorithm is employed to solve the

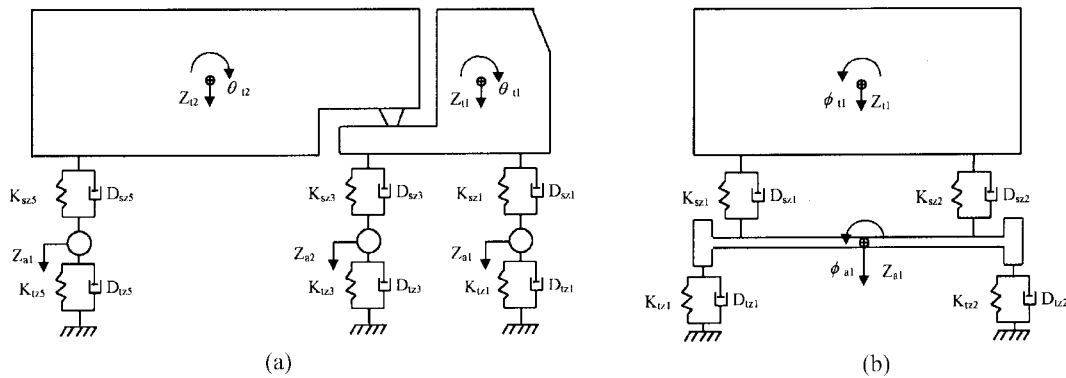


Fig. 4 HS20-44 vehicle model: (a) side view; and (b) front view

nonlinear equations of motion of vehicle (Chu *et al.* 1986, Wang 1990, Wang *et al.* 1991). The dynamic equations of the bridge are solved by the modal superposition procedure based on the subspace iteration method.

4. Road surface roughness

Dodds and Robson (1973) have developed the power spectral density (PSD) functions for highway surface roughness:

$$S(\bar{\phi}) = \begin{cases} A(\bar{\phi}/\bar{\phi}_0)^{-\bar{w}_1} & \bar{\phi} \leq \bar{\phi}_0 \\ A(\bar{\phi}/\bar{\phi}_0)^{-\bar{w}_2} & \bar{\phi} > \bar{\phi}_0 \end{cases} \quad (4)$$

where $S(\bar{\phi})$ = PSD ($\text{m}^2/\text{cycle}/\text{m}$); $\bar{\phi}$ = wave number (cycle/m); $\bar{\phi}_0$ = discontinuity frequency = $1/2\pi$ (cycle/m); A = roughness coefficient (m^3/cycle); and \bar{w}_1, \bar{w}_2 = roughness exponent, herein taken as 2.050 and 1.440, respectively, for principal roads.

Eq. (4) presents the characteristics of road surface roughness along the longitudinal direction (x). Wang and Huang (1992) modified the spectrum by using $\bar{w}_1 = \bar{w}_2 = -2.0$, which underestimates the amplitude of those components at frequencies higher than $\bar{\phi}_0$. This modification makes little difference in the generated roughness. According to the roughness coefficient A , four classes of road surface conditions (very good, good, average, and poor) are generated by Wang and Huang (1992). In actuality, these random processes are correlated with each other along the transverse direction (y). To reflect the spatial correlation along the transverse direction, an approximate formula proposed by Kovacs and Svensson (1992) is adopted to simulate multi-correlated processes based on a given spatially correlated relationship:

$$u_{sr}(x, y_g) = \sum_{j=1}^n \sqrt{\frac{2S(\bar{\phi}_j)\Delta\bar{\phi}}{\sum_{k=1}^m C^2(\eta_k)}} \cdot \sum_{k=1}^m C(y_g - \eta_k) \cdot \cos[(\omega_j + \omega_j')x + \phi_{kj}] \quad (5)$$

where $S(\bar{\phi}_j)$ = target PSD at discrete frequency $\bar{\phi}_j$; $C(\xi)$ = transverse spatial coherence function; ξ = distance between two correlated points; η_k = lateral coordinates of a set of selected points to generate road roughness, $k = 1, \dots, m$; y_g = lateral coordinate of generated point; $\omega_j = 2\pi\bar{\phi}_j$, circular frequency; ω_j' = random circular frequency introduced hereby to avoid the periodicity of generated random process ($\omega_j' \ll \omega_j$); and ϕ_{kj} = initial phase.

Eq. (5) is initially employed to simulate spatially correlated turbulent components of natural wind along the span of large-scale bridges such as cable-stayed bridges. It demonstrates satisfactory results (Liu 1995). To appropriately use Eq. (5), it is necessary to select a set of points $\eta_k (k=1, \dots, m)$ distributed along the transverse direction. The point at which longitudinal road surface roughness is generated is supposed to be spatially correlated with these selected points as shown in Fig. 5. In this study, two parameters m and n are chosen as 10 and 200, respectively, to generate two correlated longitudinal surface roughness profiles according to a given correlation length $\bar{\theta}$. A triangle correlation model is taken to approximately reflect the spatial correlation of multi-correlated road surface roughness:

$$C(\xi) = \begin{cases} 1 - |\xi|/\bar{\theta} & \text{if } |\xi| \leq \bar{\theta} \\ 0 & \text{if } |\xi| > \bar{\theta} \end{cases} \quad (6)$$

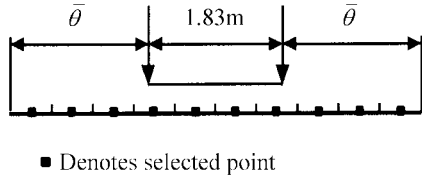


Fig 5 Indication of selected points η_k

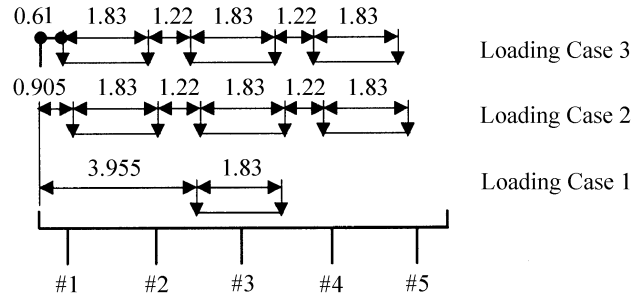


Fig 6 Truck loading model

where $\bar{\theta}$ =correlation length, which stands for the rate at which the correlation decays between two points along y-axis (transverse) direction.

In Eqs. (5) and (6), the sample length is taken as 256 m and 2048 (2^{11}) data points are generated for this length. The average and upper limit of road profile amplitude ranges for four roughness classes ($A = 5 \times 10^{-6}$, 20×10^{-6} , 80×10^{-6} , and 320×10^{-6}) are shown in Table 2.

5. Analytical study

In this study, several premises have been made as follows: (1) To simulate the vehicle entering the bridge with nonzero initial displacements and velocities at every DOF, the vehicle is started at a distance of 42.67 m, i.e., a five-car length, away from the left end of the bridge; (2) For the bridge structural damping characteristics, one percent of critical damping is adopted for the first and second modes according to the experimental results (Ruhl 1974). The modal damping coefficients are determined by using an approach described by Clough and Penzien (1996); (3) Both approach roadways and bridge decks have the same class of road surface; and (4) The left- and right-line wheelpaths have different but correlated road surface roughness characteristics. This correlation has been modeled as triangle type defined by Eq. (6). In case of multi-truck presence, trucks in different lanes have the same set of two wheelpaths, i.e., lane-to-lane differences are neglected.

A total of twenty simulations of surface roughness by Eq. (5) is performed and labeled in the number sequence of one to twenty in order to obtain statistical data. Every study case related to vehicle speed and road surface class includes twenty simulations namely a group. To present probability-based results, the smaller of the following is used in each group: (1) the maximum impact factor; or (2) the average plus 1.645 standard deviations of impact factors calculated. Since the variation of impact factors within a group could be represented by a normal distribution, the use

Table 2 Amplitude of generated road profiles

Class (1)	Very good (2)		Good (3)		Average (4)		Poor (5)	
	Left-line	Right-line	Left-line	Right-line	Left-line	Right-line	Left-line	Right-line
Average (m)	0.020	0.020	0.039	0.040	0.079	0.081	0.158	0.161
Upper limit of 95% confidence level (m)	0.025	0.026	0.051	0.051	0.102	0.103	0.204	0.205

of average plus 1.645 standard deviations assures that the assigned impact factors to a group have only a 5 percent chance of being exceeded.

For the analytical bridge, the specified values are 22 percent for impact factor according to AASHTO specifications (1996) and 0.33 for dynamic load allowance (strength limit states of girders) according to AASHTO-LRFD specifications (1998).

5.1 Statistics of impact factors

Following the design loading of the bridge, loading cases 2 and 3 in Fig. 6 are adopted to analyze the dynamic behavior of the bridge. The symmetric and asymmetric three-truck loading cases (loading cases 2 and 3) are used for center girder and two exterior girders, respectively. To obtain statistical results of dynamic responses, a total of 20 sets of road surface roughness is generated by Eq. (5), and the correlation length $\bar{\theta}$ is taken as 5 m (roughly half the bridge width). The amplitude ranges of twenty simulated left- and right-line profile differences fall within the range from 0.022 to 0.042 m, while the measured difference for Big Sandy Bridge by Law *et al.* (1975) are in the range from 0.020 to 0.036 m (the road surface condition is good). Thus, the selection of correlation length $\bar{\theta} = 5$ m is appropriate. The calculated left- and right-line profile difference of roughness #1 according to $\bar{\theta} = 5$ m is shown in Fig. 7.

The impact factor is defined as the following:

$$I_{mp}(\%) = \left(\frac{R_d}{R_s} - 1 \right) \times 100\% \quad (7)$$

where R_d and R_s = the absolute maximum dynamic and static responses for individual histories, respectively.

Tables 3-6 present the variation of the upper limits of moment impact factors (confidence level of 95 percent) at midspan of five girders with various vehicle speeds (ranging from 24.14 to 120.70 km/h) and different classes of road surface roughness. The following concepts can be learned from Tables 3-6. Two exterior girders #1 and #5 have the largest impact factors, while the central girder #3 is subjected to the intermediate impacts. The moment impact factors tremendously increase with the surface roughness class in the sequence from very good to poor. For very good road surface, all impact factors safely fall within the specified value of AASHTO specifications (1996); however, all impact factors exceed the specified value for the average and poor classes. At various vehicle speeds, the impact factors of each girder appear to be different. For good road surface, the AASHTO specifications (1996) cover the upper limits under confidence level of 95 percent when vehicle speed is less than 104.60 km/h. Although the upper limits are higher than the specified value of 22 percent when vehicle speed reaches 120.70 km/h, all of them are smaller than the specified dynamic load allowance of 0.33 (AASHTO-LRFD 1998). Based on these results, the following study will focus on the dynamic behaviors of the bridge with very good and good road surfaces.

A typical distribution of impact factors within a group is illustrated in Fig. 8. It can be noticed from Fig. 8 that the diversity of computed impact factors within a group are apparent. The phenomenon indicates that the inputs of various road roughness having the same power density spectrum, affect initial displacements and velocities of vehicle DOFs and vehicle-bridge interaction. This means that impact factors are random variables. Table 7 gives the results based on single simulation of good road surface and its modified PSD by Wang *et al.* (1992) and Huang *et al.* (1993). By comparing Table 7 with Table 4, it can be seen that the predicted upper limits under confidence level of 95 percent appear to be much higher. Hence, it is necessary to compute the

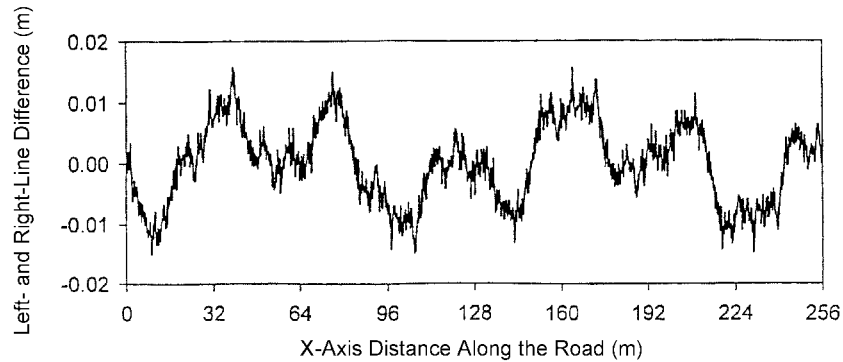


Fig. 7 Left-and right-line profile difference on good surface roughness #1($\bar{\theta} = 5$ m)

Table 3 Moment impact factors at midspan (very good road surface)

Speed (km/h) (1)	Girder 1 (2)	Girder 2 (3)	Girder 3 (4)	Girder 4 (5)	Girder 5 (6)
24.14	7.493	4.955	6.967	5.071	7.925
40.23	8.017	5.300	7.135	5.159	7.977
56.33	8.007	5.512	7.487	5.543	8.225
72.42	7.186	4.472	6.516	4.758	7.691
88.51	7.153	4.586	6.288	3.923	6.460
104.60	9.342	7.057	9.119	7.106	9.441
120.70	14.957	12.454	14.543	12.541	14.752

Table 4 Moment impact factors at midspan (good road surface)

Speed (km/h) (1)	Girder 1 (2)	Girder 2 (3)	Girder 3 (4)	Girder 4 (5)	Girder 5 (6)
24.14	17.024	13.847	16.211	14.091	17.783
40.23	16.663	12.752	14.932	13.053	17.607
56.33	17.033	14.749	17.012	14.881	17.996
72.42	14.789	11.334	13.658	11.756	16.000
88.51	12.851	9.928	11.875	9.312	10.875
104.60	17.804	14.391	16.595	14.460	17.912
120.70	28.803	26.293	28.457	25.553	27.868

upper limits under a specific confidence level based on statistical results.

Fig. 9 presents the calculated upper limits of impact factors under very good and good road conditions and confidence level of 95 percent in comparison with AASHTO specifications. From Fig. 9, it can be observed that all impact factors under very good road condition are less than the specified value by AASHTO specifications (1996). Under good road conditions, the impact factors of the center girder #3 are less than the specified value by AASHTO specifications (1996), except the moment impact factor at midspan based on the highest speed of 120.70 km/h; the moment impact factors at midspan of the exterior girder #1 are similar to those of the center girder #3. Moreover, the moment impact factors at quarter point of the exterior girder #1 are generally less than the specified value by AASHTO specifications (1996), while most of shear impact factors at

Table 5 Moment impact factors at midspan (average road surface)

Speed (km/h) (1)	Girder 1 (2)	Girder 2 (3)	Girder 3 (4)	Girder 4 (5)	Girder 5 (6)
24.14	43.678	39.015	47.188	38.933	43.782
40.23	43.450	37.385	39.314	35.599	39.179
56.33	42.139	37.505	39.939	37.352	43.538
72.42	36.900	31.950	34.260	31.923	37.592
88.51	30.837	28.010	31.622	28.709	29.790
104.60	49.216	43.034	46.166	42.718	48.514
120.70	64.005	58.254	61.395	58.287	63.565

Table 6. Moment impact factors at midspan (poor road surface)

Speed (km/h) (1)	Girder 1 (2)	Girder 2 (3)	Girder 3 (4)	Girder 4 (5)	Girder 5 (6)
24.14	125.718	115.837	122.021	118.896	130.200
40.23	109.023	101.089	105.938	102.841	113.489
56.33	111.210	102.057	106.074	103.121	116.825
72.42	84.994	78.433	83.327	82.951	93.226
88.51	116.845	111.393	120.030	118.909	131.811
104.60	158.653	142.778	147.650	144.749	158.933
120.70	139.216	129.075	133.189	127.398	140.364

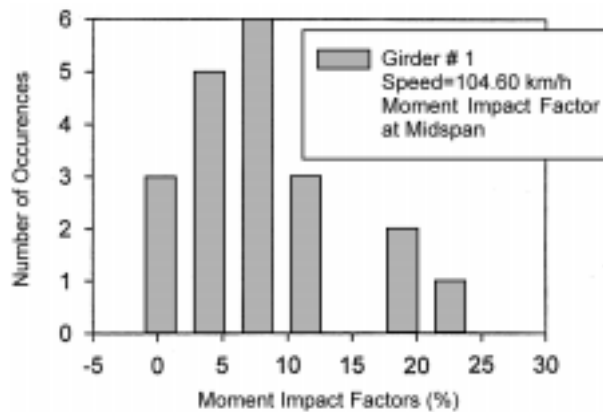


Fig. 8 Typical impact factor distribution

end exceed the specified value by AASHTO specifications (1996). All impact factors are less than the specified dynamic load allowance IM by AASHTO-LRFD specifications (1998). One lowermost point occurs for all curves within the vehicle speeds from 72.42 to 88.51 km/h because of the smallest averages and standard deviations.

5.2 Effect of correlation length

In order to study the influence of correlation length $\bar{\theta}$ on dynamic impact factors, a variety of

Table 7 Moment impact factors at midspan (good road surface and modified PSD)

Speed (km/h) (1)	Girder 1 (2)	Girder 2 (3)	Girder 3 (4)	Girder 4 (5)	Girder 5 (6)
24.14	2.581	1.097	2.803	1.215	3.814
40.23	4.053	1.029	3.232	1.617	4.824
56.33	4.566	1.828	3.999	1.810	5.547
72.42	3.253	1.762	3.983	2.422	4.264
88.51	5.709	3.543	5.657	3.670	5.608
104.60	8.180	6.357	8.441	6.404	8.444
120.70	13.130	10.750	13.060	11.630	15.200

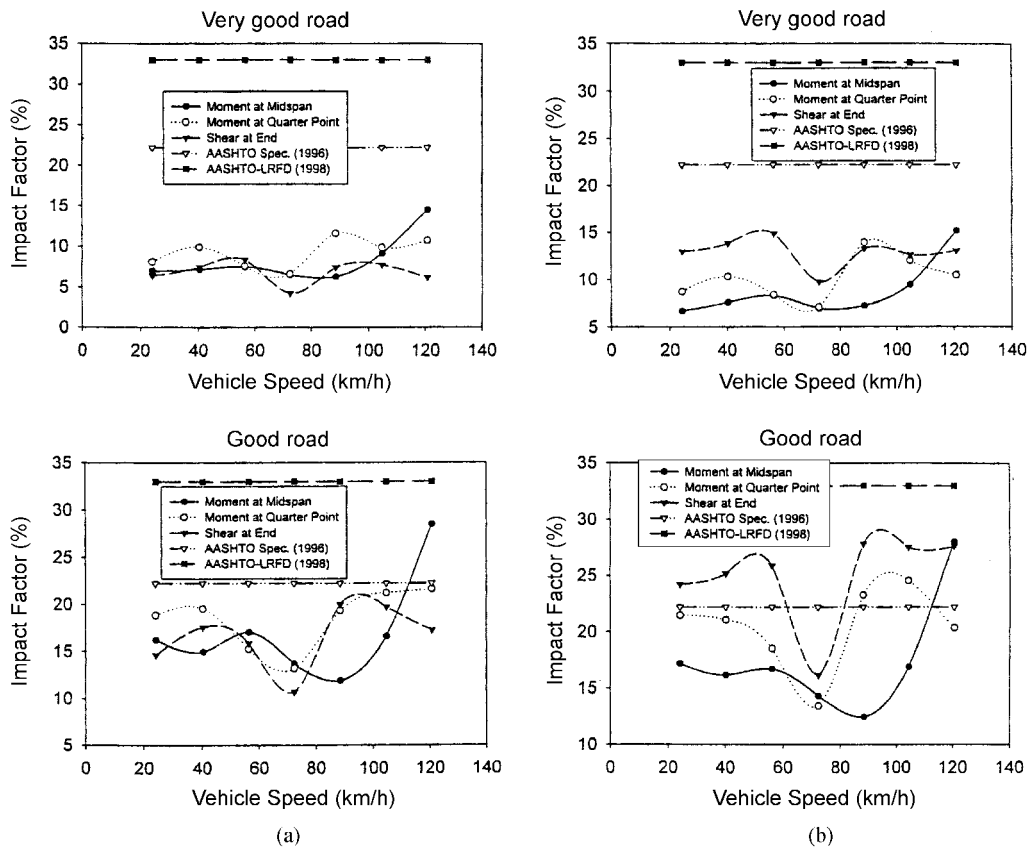


Fig. 9 Variation of impact factors with vehicle speed: (a) center girder #3; and (b) exterior girder #1

correlation length $\bar{\theta}$ (5 m to 1000 m) in Eq. (6) is taken to generate twenty sets of spatially correlated road surface roughness that are supposed to stationary and ergodic processes. It is observed that there is somewhat discrepancy between the correlation coefficient of simulated roughness profiles and that defined by Eq. (6) when the correlation coefficient is small. Herein, those correlation lengths $\bar{\theta}$ less than 5 m are not used to avoid such a situation. At each fixed longitudinal point x_i ($i=1, \dots, 2^{11}$), the left- and right-line roughness $u_{sr}(x_i, y_l)$ and $u_{sr}(x_i, y_r)$ are two correlated random variables with zero mean value. The correlation of the two variables is

examined by the following:

$$\hat{\rho}_i = \sum_{j=1}^{n_s} (u_{lj} - \bar{u}_l)(u_{rj} - \bar{u}_r) / n_s \sigma_{u_l} \sigma_{u_r} \quad (8)$$

where $\hat{\rho}_i$ = estimated correlation coefficient of left- and right-lines u_l and u_r at step; u_{lj} and u_{rj} = left- and right-lines, $u_{sr}(x_i, y_l)$ and $u_{sr}(x_i, y_r)$, at the j th simulation; \bar{u}_l and \bar{u}_r = average values of u_{lj} and u_{rj} , and theoretically they approach zero if n_s approaches infinite; y_l and y_r = lateral coordinates of generated left- and right-lines; σ_{u_l} , σ_{u_r} = standard deviations of left- and right-lines u_l and u_r , respectively; and $n_s = 20$, number of simulation times.

The statistics of estimated coefficient of correlation by Eq. (8) are calculated on the basis of 2048 (2^{11}) data points of good road surfaces. The comparison between statistical results and theoretical correlation coefficients is listed in Table 8. From Table 8, it can be seen that the results generated by Eq. (5) are satisfactory under the given values of $\bar{\theta}$.

Fig. 10 illustrates the generated left- and right-lines of road surface roughness #5 for $\bar{\theta} = 5$ m and $\bar{\theta} = 20$ m. These two correlation lengths turn out to be two sets of road surfaces with different characteristics. The larger correlation length ensures a better coherence between the left- and right-line roughness.

Structural dynamic responses at midspan for the symmetric one-truck loading case 1 (see Fig. 6) are calculated on the basis of 72.42 km/h vehicle speed and good road surface. Table 9 illustrates the variation of impact factors with correlation length $\bar{\theta}$ given four pairs of individual road surface roughness #1, #5, #10, and #14. The results indicate that moment impact factors at midspan basically increase with $\bar{\theta}$ for all five girders. In other words, the better the correlation between two road surface roughness profiles is, the larger the consequent impact effects will be. Nevertheless, the increments of impact factors in the center girder subject to the maximum static stresses are small, usually around 0.02.

The preceding comparison is based on individual response histories. To further obtain the possible discrepancy between different correlation lengths, it is necessary to calculate statistical data and analyze the difference. Loading case 2 in Fig. 6 is adopted to analyze the dynamic behavior of the bridge. The upper limits of moment impact factors at midspan under confidence level of 95 percent and $\bar{\theta} = 1000$ m are computed twenty times on good road surface at the vehicle speeds ranging

Table 8 Comparison of correlation coefficient

Correlation length $\bar{\theta}$ (m) (1)	Estimated correlation coefficient $\hat{\rho}_{u_r, u_l}^a$ (2)	Theoretical correlation coefficient ρ_{u_r, u_l}^b (3)	Error ^c (%) (4)
5	0.682 0.123	0.634	7.6
10	0.812 0.078	0.817	-0.6
20	0.948 0.024	0.909	4.3
1000	1.000 0.000	0.998	0.2

Note: ^a. Upper numbers denote average values and the lower numbers denote standard deviations the coefficient is computed by Eq. (8), ^b. The coefficient is computed by Eq. (6), and ^c. Compared with estimated average values only

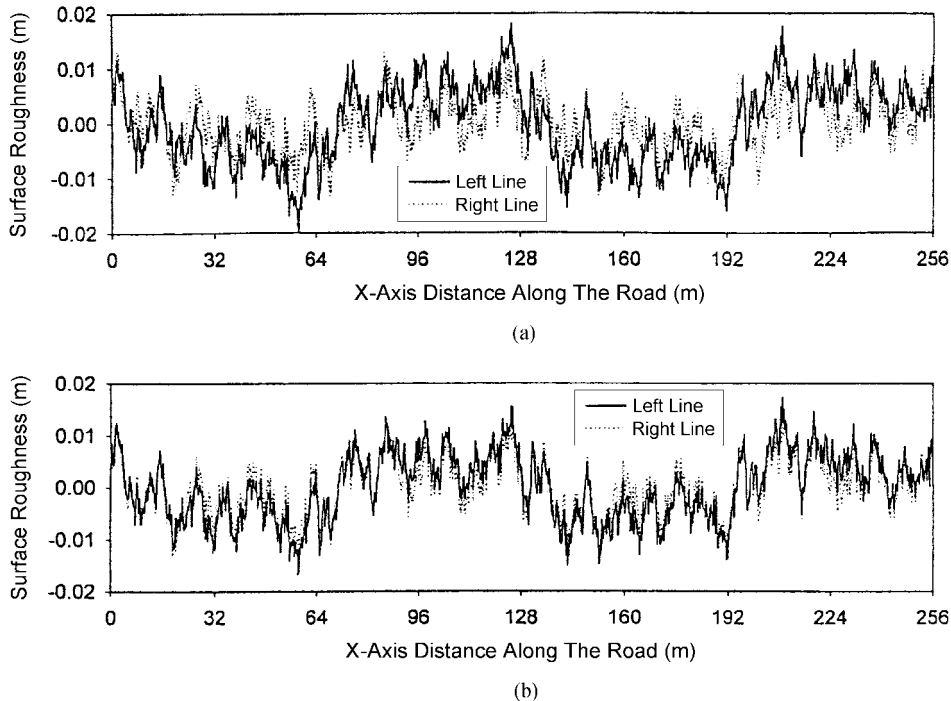


Fig. 10 Left- and right-lines of road surface roughness #5: (a) $\bar{\theta} = 5$ m; and (b) $\bar{\theta} = 20$ m

from 24.14 to 120.70 km/h as shown in Table 10. The purpose of the selection of $\bar{\theta} = 1000$ m is to obtain completely the same left- and right-line roughness. By comparing Table 10 with Table 4, the following trends can be observed that: (1) a better correlation between road surface roughness results in larger impact factors and these increments of impact factors are generally around 0.02; and (2) similar to those of $\bar{\theta} = 5$ m, the upper limits of $\bar{\theta} = 1000$ m are generally less than the specified value of AASHTO specifications (1996) except the case at the highest vehicle speed of 120.70 km/h.

6. Conclusions

In general, the vehicle-induced impact of bridge is highly related to the road surface roughness. Utilizing the established three-dimensional vehicle model in the previous study, it is rational to generate longitudinal road surface roughness as multi-correlated random processes along deck transverse direction. In this study, a triangle correlation model is used to approximately describe the lateral spatial coherence.

The advantage of statistical analysis of impact factors obviously lies in that it can predict upper limits (possible maximum impact factors) under a given confidence level. In the example, twenty simulations are carried out as a group for each study case and the prediction based on confidence level of 95 percent but no more than the maximum value within each group is taken. The comparison with results from single simulation indicates that the results from two methods are distinct. Therefore, it is necessary to predict the upper limits based on a set of simulated road roughness.

The impact factors tremendously increase with the surface roughness class in the sequence from

Table 9 Variation of impact factors with $\bar{\theta}$

Correlation Length $\bar{\theta}$ (m) (1)	Girder # 1 (2)	Girder # 2 (3)	Girder # 3 (4)	Girder # 4 (5)	Girder # 5 (6)
5	24.880 ^a	15.840	9.508	17.840	27.300
	6.141 ^b	0.123	-3.372	1.565	7.796
	10.440 ^c	4.406	-0.714	6.072	11.990
	11.730 ^d	10.830	5.800	10.610	11.550
10	27.150	17.910	10.86	19.150	28.260
	7.279	2.082	-1.811	2.771	8.189
	8.984	4.029	-1.183	5.121	9.533
	13.540	12.500	7.280	12.250	13.280
20	29.230	19.470	11.940	20.190	29.780
	8.581	2.770	-1.638	3.016	8.752
	10.200	5.059	-0.412	5.499	10.460
	14.700	13.320	8.371	13.000	14.140

Note: ^a. road surface roughness #1, ^b. road surface roughness #5, ^c. road surface roughness #10; ^d. road surface roughness #14; and so on

Table 10 Moment impact factors at midspan (good road surface and $\bar{\theta} = 1000$ m)

Speed (km/h) (1)	Girder 1 (2)	Girder 2 (3)	Girder 3 (4)	Girder 4 (5)	Girder 5 (6)
24.14	19.439	15.526	17.773	15.809	19.690
40.23	18.328	14.070	16.385	14.132	18.271
56.33	19.125	16.012	18.124	15.913	18.682
72.42	16.637	12.920	15.127	12.820	16.634
88.51	12.080	10.524	12.926	10.708	12.271
104.60	18.234	15.563	17.778	15.625	18.568
120.70	31.415	28.284	30.370	28.123	31.124

very good to poor. For very good roads, all upper limits of impact effects are less than the specified value by AASHTO specifications (1996), but are apparently greater than the specified value for average and poor roads. In the case of good roads, the upper limits of impact factors under 95 percent confidence level fluctuate around the specified value.

At various vehicle speeds, the upper limits of impact factors of all girders appear to be different. The maximum impacts basically occur at the high vehicle speeds over 88.51 km/h. Given good road condition, impact factors of center girder #3 are in accordance with the AASHTO specifications (1996), except the moment impact factors at the highest speed of 120.70 km/h; for the exterior girders #1 and #5, most of the shear impact factors at end and a few moment impact factors at quarter point at high vehicle speeds exceed the specified value of AASHTO specifications (1996). However, all upper limits are less than the specified dynamic load allowance by AASHTO-LRFD (1998).

The influence of correlation of two-wheel-line road surface roughness on impact is investigated on two levels: individual response history and upper limits based on statistical data. From individual response histories, which are obtained under symmetric one-truck loading, it is observed that the moment impact factor at all five girders generally increases with correlation length $\bar{\theta}$. From the statistical results with confidence level of 95 percent, a better correlation between two road roughness profiles consequently results in larger impact effects. The moment impact factors at midspan indicate that the increments of impact factors in the center girder #3 with maximum static stresses are not of significance, usually around 0.02, among various values of $\bar{\theta}$. The aforementioned

tendencies are observed only from the bridge with a span of 30.48 m. For other bridges with different spans, this needs further investigation.

Based on the theoretical studies, two measures in bridge management are recommended to avoid severe impact damage by moving vehicles: (1) reducing the roughness of road surface as much as possible, e.g., to meet the requirement of good road surface or better; and (2) regulating passing speeds of heavy trucks to those less than 88.51 km/h. Since the upper limits of shear impacts at end of exterior girders are generally higher than others on good road condition and exceed the specified value by AASHTO specifications (1996), it is emphasized of practical importance to examine the relevant systems, such as bearing systems of two exterior girders in routine maintenance of this type of bridges.

References

- AASHTO (1996), *Standard Specifications for Highway Bridges*, 16th Ed., American Association of State Highway and Transportation Officials, Washington, D. C.
- AASHTO (1998), *LRFD Bridge Design Specifications-Customary U.S. Units*, 2nd Edition, Am. Assoc. of State Hwy. And Transp. Officials (AASHTO), Washington, D. C.
- Chu, K.H., Garg, V.K. and Wang, T.L. (1986), "Impact in railway prestressed concrete bridges", *J. Struct. Engrg.*, ASCE, **116**(7), 1036-1051.
- Clough, R.W. and Penzien, J. (1996), *Dynamics of Structures*, McGraw-Hill Book Co., 2nd Ed., New York, N.Y.
- Dodds, C.J. and Robson, J.D. (1973), "The description of road surface roughness", *Journal of Sound and Vibration*, **31**(2), November, 175-183.
- Fenves, S.J., Veletsos, A.S., and Siess, C.P. (1962), "Dynamic studies of bridges on the AASHTO test road", Report No. 71, Nat. Academy of Sci.-Nat. Res. Council, Washington, D. C.
- Huang, D.Z., Wang, T.L. and and Shahawy, M. (1993), "Impact studies of multigirder concrete bridges", *J. Struct. Engrg.*, ASCE, **119**(8), 2387-2402.
- Kovacs, I., Svensson, H. and Jordet, E. (1992), "Analytical aerodynamic investigation of cable-stayed Helgeland bridge", *J. Struct. Engrg.*, ASCE, **118**(1), 147-168.
- Law, D.B., Williamson, H.J. and Hudson, W.R. (1975), "The characterization of road roughness on bridge decks and the adjoining pavement", Research Report No. FHWA-RD-75-SO409, Texas Highway Dept., Planning & Research Division, Austin, Texas.
- Liu, C.H. (1995), "Nonlinear time-domain analysis of buffeting for long span bridges", Ph.D. dissertation, Tongji University, Shanghai, P. R. China.
- Ruhl, J. (1974), "Stress histories for highway bridges subjected to traffic loading", Ph.D. dissertation, University of Illinois, Urbana, Ill.
- Wang, T.L. (1990), "Ramp/bridge interface in railway prestressed concrete bridges", *J. Struct. Engrg.*, ASCE, **116**(6), 1648-1659.
- Wang, T.L., Garg, V.K. and Chu, K.H. (1991), "Railway bridge/vehicle interaction studies with a new vehicle model", *J. Struct. Engrg.*, ASCE, **117**(7), 2099-2116.
- Wang, T.L. and Huang, D.Z. (1992), "Computer modeling analysis in bridge evaluation", Research Report No. FL/DOT/RMC/0542-3394, Florida Dept. of Transp., Tallahassee, Fla.
- Wang, T.L., Huang D.Z. and Shahawy, M. (1992), "Dynamic response of multigirder bridges", *J. Struct. Engrg.*, ASCE, **118**(8), 2222-2238.
- Wang, T.L., Huang D.Z. and Shahawy, M. (1993), "Vibration and impact in multigirder steel bridges", Transp. Research Record, Transp. Research Board (TRB), National Research Council, Washinton, D.C., No. 1393, Aug., 96-103.
- Wang, T.L. *et al.* (1996), "Dynamic response of highway girder bridges", *International J. of Computers and Structures*, **60**(6), 1021-1027.
- U.S. Dept. Of Transp. (1990), *Standard Plans for Highway Bridge Superstructures*, Federal Highway Admin., Washington, D. C.